Leaky-Wave Antennas Based on Noncutoff Substrate Integrated Waveguide Supporting Beam Scanning From Backward to Forward

Yue-Long Lyu, *Student Member, IEEE*, Xiao-Xin Liu, Peng-Yuan Wang, Daniel Erni, *Member, IEEE*, Qun Wu, *Senior Member, IEEE*, Cong Wang, *Senior Member, IEEE*, Nam-Young Kim, *Member, IEEE*, and Fan-Yi Meng, *Senior Member, IEEE*

***Abstract*—In this paper, we propose an approach to realize substrate integrated waveguide (SIW)-based leaky-wave antennas (LWAs) supporting continuous beam scanning from backward to forward above the cutoff frequency. First, through phase delay analysis, it was found that SIWs with straight transverse slots support backward and forward radiation of the -1-order mode with an open-stopband (OSB) in between. Subsequently, by introducing additional longitudinal slots as parallel components, the OSB can be suppressed, leading to continuous beam scanning at least from -40° through broadside to 35°. The proposed method only requires a planar structure and obtains less dispersive beam scanning compared with a composite right/left-handed (CRLH) LWA. Both simulations and measurements verify the intended beam scanning operation while verifying the underlying theory.**

***Index Terms*—Backward radiation, broadside radiation, forward radiation, leaky-wave antenna (LWA), open-stopband (OSB).**

I. Introduction

A LEAKY-WAVE antenna (LWA) refers to a type of traveling-wave structure based on a transmission line loaded with radiating elements [1]. They were first designed using a rectangular waveguide with slots [2]. The arrangement of the slots determines the polarization and the radiation direction of the LWA [3]. Periodic loading of the same components on each unit cell of the LWA leads to a high directivity, and a frequency-dependent beam scanning ability. These unique characteristics make the LWA attractive in many applications such as frequency modulated continuous wave radar [4], real-time spectrum analysis [5], and field pattern synthesis [6].

The beam scanning range is one of the most concerned issues in LWA design. Early LWAs radiate electromagnetic (EM) power only forward (toward end-fire) as frequency goes up [7]–[9], or both forward and backward (i.e., backfire) but not broadside, which is due to the open-stopband (OSB) effect [10], [11]. In [12], the OSB is attributed to the unmatched unit cell structure of LWAs. At the frequency of broadside radiation, the reflected waves of each unit cell are in phase, and hence no EM power is fed into the LWA for broadside radiation. To obtain seamless beam scanning from backward to forward, a few types of microstrip LWAs have been proposed to suppress the OSB by means of reflection cancellation [12], impedance matching [12], [13], and implementing asymmetric unit cells [14], [15]. On the other hand, the continuous beam scanning of LWA can also be achieved by making use of the concept of balanced composite right/left-handed (CRLH) transmission line [16]. In the past decade, varieties of CRLH-based LWAs were designed utilizing microstrip lines [17], mushroom structures [18], [19], coplanar striplines [20], coplanar waveguides [21], [22], rectangular waveguides [23]–[25], and substrate integrated waveguides (SIWs) [26]–[28]. Among all these waveguide topologies rectangular waveguide and SIW-based LWAs have demonstrated their advantages such as low loss and high-power capacity. However, most of the SIW or rectangular waveguide-based CRLH LWAs operate from below the cutoff frequency [4], [24], [27]. This is because cutoff rectangular waveguides and SIWs possess inherent shunt inductances, which is constitutive for realizing CRLH transmission lines. However, such CRLH LWA is usually hard to match due to the highly dispersive nature of the cutoff waveguide [24], [27]. CRLH LWAs above the cutoff frequency have been proposed in [25] using a rectangular waveguide with inductive irises, but this LWA is bulky and relies on complex 3-D structures, which are hard to fabricate.

Very recently, some SIW-based LWAs have been designed to operate above the cut-off frequency such as the LWA with long slots [29], [30], and the forward radiating LWA with transverse slots as presented in [31]–[33]. However, the LWAs in [29] and [30] require ridges to achieve backward, broadside, and forward radiation, relying on multilayer substrates for fabrication

Manuscript received September 08, 2015; revised March 25, 2016; accepted March 29, 2016. Date of publication April 04, 2016; date of current version May 30, 2016. This work was supported part by the Open Project Program of the State Key Laboratory of Millimeter Wave under Grant K201403. *(Corresponding author: Fan-Yi Meng.)*

Y.-L. Lyu and P.-Y. Wang are with the Department of Engineering, Harbin Institute of Technology, Harbin 150001, China (e-mail: lvyuelonglvyuelong@126.com; pywang@hit.edu.cn).

X.-X. Liu is with Beijing Aerospace Microsystems Institute, Beijing 100094, China (e-mail: liuxiaoxin_0014pm@163.com).

D. Erni is with the Faculty of Engineering, Laboratory for General and Theoretical Electrical Engineering (ATE), CENIDE—Center for Nanointegration Duisburg-Essen, University of Duisburg-Essen, D-47048 Duisburg, Germany (e-mail: daniel.erni@uni-due.de).

Q. Wu and F.-Y. Meng are with the Department of Microwave Engineering, Harbin Institute of Technology, Harbin 150001, China, and also with the State Key Laboratory of Millimeter Waves, Nanjing 210096, China (e-mail: blade@hit.edu.cn; qwu@hit.edu.cn).

C. Wang and N.-Y. Kim are with the Department of Wireless Communication Engineering, Kwangwoon University, Seoul 139-701, South Korea (e-mail: kevin_wang@kw.ac.kr; nykim@kw.ac.kr).

Color versions of one or more of the figures in this paper are available online at http://ieeexplore.ieee.org.

Digital Object Identifier 10.1109/TAP.2016.2550054

purposes. Furthermore, the LWAs in [31]–[33] are not able to realize broadside radiation due to the OSB as will be discussed later in this paper. Although the OSB can be suppressed in LWAs consisting of reflection-canceling transverse slot pairs [34], [35], this type of LWAs usually radiates linearly polarized EM waves with their polarization directions along the longitudinal axis of the SIW. Radiation of other polarizations requires adaption of the transverse slot pair. For example, an oblique slot is added between the transverse slot pair to achieve 45° linear polarization [36]. In this paper, we propose a LWA design method to suppress the OSB by an impedance-matched LWA unit cell. The required unit cell consists of both transverse and longitudinal slots on the top layer of the SIW as the series and shunt loading elements, respectively. By careful design, a series of LWAs are realized capable of EM wave emission with a seamless transition through broadside. The proposed LWAs are easy to fabricate owing to its single-layer structure. In addition, the proposed LWAs in this paper radiate linear polarized EM waves with polarization directions perpendicular to the longitudinal axis of the SIW. However, they are also promising for circularly polarized radiation as shown later. A prototype of the proposed LWAs is fabricated and experimentally validated as proof of concept where the measured results agree perfectly well with the simulated data.

This paper is organized as follows. Section II provides a discussion on SIW LWAs with transverse slots, aiming at providing a theoretical foundation of the underlying radiation properties, whereas Section III gives the theoretical description, the model design, and optimization of the new planar structure with both transverse and longitudinal slots for continuous beam scanning through broadside. Section IV presents the measurement of a fabricated prototype. Finally, Section V concludes this paper.

II. SIW-Based LWA With Transverse Slots

The structure of the SIW-based LWA with transverse slots is sketched in Fig. 1(a), which is a similar structure as discussed in [31]. The substrate is covered with copper on both sides forming a waveguide, together with two rows of metallic vias along the wave propagation direction. The thickness and the width of the SIW are h and w, respectively. The diameter of the metallic vias is d, and the period of the vias is s. For the following theoretical analysis including numerical simulations conducted with the CST MWS software package, the SIW is simplified to a flattened dielectric-filled rectangular waveguide with an effective width w_{eff} as obtained from [37] to reduce both the numerical complexity and simulation time [as shown in Fig. 1(b)]. In this simplified case, for the TE_{10} mode, the phase constant β can be written as following, where the relative permittivity of the substrate is $\varepsilon_r = 3.66$:

$$\beta = \sqrt{\varepsilon_r {k_0}^2 - \left(\frac{\pi}{w_{eff}}\right)^2}. \tag{1}$$

The transverse slots on the top of the SIW are implemented to perturb the current distribution, not only for radiating EM power to the free space, but also for introducing an additional

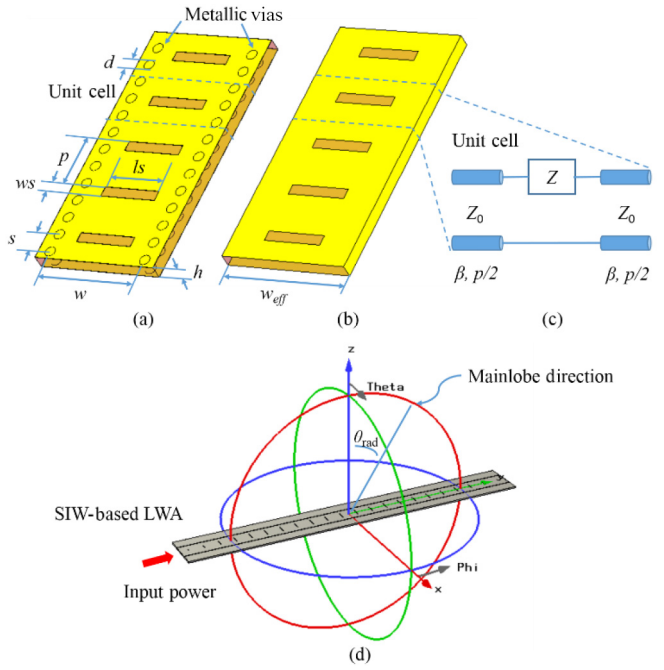

Fig. 1. Structure of the SIW-based LWA with transverse slots: (a) realized model; (b) rectangular waveguide model for simulation purposes; (c) equivalent circuit of the unit cell; and (d) LWA alignment in the coordinates.

phase delay in the underlying transmission line. The width, length, and period of the slots are *ws*, *ls*, and p, respectively. The unit cell of the LWA is modeled with two transmission line segments and a series loaded impedance in between as sketched in Fig. 1(c). Its S parameters can be described as follows:

$$\mathrm{S}_{unit} = \begin{pmatrix} \dfrac{Z/Z_0}{2+Z/Z_0} e^{-j\beta p} & \dfrac{2}{2+Z/Z_0} e^{-j\beta p} \\ \dfrac{2}{2+Z/Z_0} e^{-j\beta p} & \dfrac{Z/Z_0}{2+Z/Z_0} e^{-j\beta p} \end{pmatrix} \tag{2}$$

where Z_0 is the port impedance and Z represents the impedance corresponding to the transverse slot. The phase increment caused by the transverse slot is $\arg(Z/Z_0+2)$. The effective phase constant β_{eff} and the attenuation constant α_{eff} of the unit cell are obtained from [21]

$$\begin{cases} |\beta_{eff}| = \dfrac{1}{p}\mathrm{Re}\left[\cos^{-1}\left(\dfrac{A+D}{2}\right)\right] \\ \alpha_{eff} = \dfrac{1}{p}\mathrm{Im}\left[\cos^{-1}\left(\dfrac{A+D}{2}\right)\right] \end{cases} \tag{3}$$

where A and D are the elements of the *ABCD* matrix of the unit cell, which can be calculated through (2) using the classic conversion formulas [38]. For the alignment of the LWA in the coordinate system shown in Fig. 1(d), the radiation direction of SIW LWA can be derived as follows:

$$\theta_{rad} = \arcsin\left(\frac{\beta_{eff}}{k_0}\right) \tag{4}$$

where k_0 is the wavenumber of free space. When $|\beta_{eff}| < k_0$, EM waves are within the fast wave regime and thus have the potential to be radiated from the LWA, otherwise the EM

TABLE I
STRUCTURE PARAMETERS OF THE SIW-BASED LWA WITH TRANSVERSE SLOTS

Parameters	w	d	s	w_{eff}	h	ws	ls	p
Values (mm)	10	0.8	1.6	10	0.762	0.45	6	15

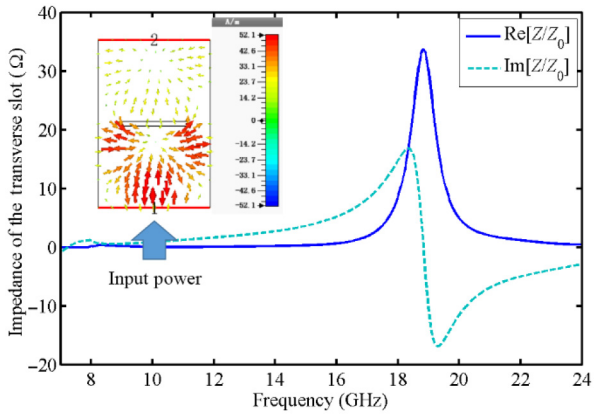

Fig. 2. Simulated impedance Z of the transverse slot normalized to the port impedance.

waves propagate as (guided) slow wave modes and cannot be radiated at all. The positive, zero, and negative values of the θ_{rad} indicate forward, broadside, and backward radiation, respectively.

Considering a parametrized SIW with transverse slots according to Table I, the impedance characteristics of the slot should be investigated first, having Z approximately described as follows:

$$Z = j\frac{1}{2}Z_e \tan\left(2\pi f\sqrt{\varepsilon_{eff}}\cdot ls/2\right) + R \tag{5}$$

where Z_0, ε_{eff}, and R are the characteristic impedance, effective permittivity, and the radiation resistance of the slot, respectively. The resonant frequency of the slot is denoted as follows:

$$f_0 = c/\left(2\sqrt{\varepsilon_{eff}}\cdot ls\right) \tag{6}$$

where c is the speed of light. Z is then extracted from the simulated S parameters of the unit cell of the SIW LWA and its frequency response is depicted in Fig. 2 when normalized to the port impedance Z_0 of the waveguide. As shown in Fig. 2, Z has an increasing positive imaginary part within a large-frequency band up to $f_0 = 18.83$ GHz, which means that the transverse slot remains inductive within this frequency range. The inset of Fig. 2 depicts the surface current distribution of the unit cell at 11.8 GHz. The phenomenon that the surface current is strong at the ends of the slot but weak at its center verifies the inductive property of the transverse slot at this frequency. On the other hand, the real part of Z [i.e., R in (5)] is relatively small except at 20.25 GHz. The phase increment $\arg(Z/Z_0 + 2)$ caused by the transverse slot is displayed in Fig. 3. The calculated $k_0 \cdot p$ and $\beta \cdot p$ and the simulated effective phase $\beta_{eff} \cdot p$ and the attenuation $\alpha_{eff} \cdot p$ of one unit cell are also shown in this figure.

In Fig. 3, one can observe three distinct radiation bands where $|\beta_{eff} \cdot p| < k_0 p$ and $\alpha_{eff} \cdot p$ is small. The corresponding

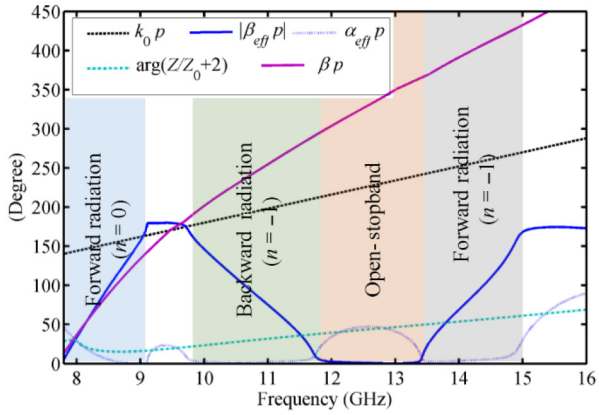

Fig. 3. Comparison of calculated $k_0 \cdot p$, simulated $|\beta_{eff} \cdot p|$ and $\alpha_{eff} \cdot p$ of the unit cell, simulated $\arg(Z/Z_0 + 2)$, and the calculated $\beta \cdot p$.

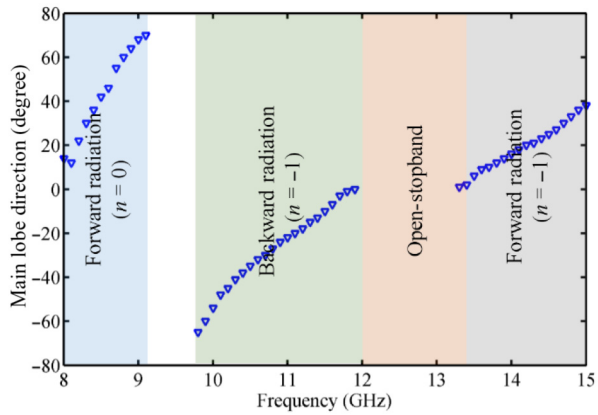

Fig. 4. Simulated mainlobe direction of the LWA consisting of 10 unit cells of different radiation modes.

mainlobe direction of a LWA constructed from cascading 10 unit cells is depicted in Fig. 4. The lower boundaries of these radiation bands are determined by the Bragg reflection condition $\beta \cdot p = m\pi$ [16], where $m = 0, 1,$ and 2, respectively. Both $\arg(Z/Z_0 + 2)$ and $\beta \cdot p$ increase in concert with the frequency and lead to an increasing $\beta_{eff} \cdot p$ too. For the $n = 0$ harmonic, $\beta_{eff} \cdot p$ rises from 0 to π in the band from the cutoff frequency of 7.9–9.1 GHz, resulting in forward beam scanning from 10° to 70° (see Fig. 4) as discussed in [33]. As the frequency continuously increases, the $n = -1$ harmonic is able to leak EM waves. The decreasing $|\beta_{eff} \cdot p|$ from 9.8 to 11.8 GHz and the increasing $|\beta_{eff} \cdot p|$ from 13.4 to 15 GHz (as depicted in Fig. 3) indicate a backward (from $-60°$ to broadside) and a forward beam scanning (from broadside to 40°), respectively. The frequency band from 11.8 to 13.4 GHz is the so-called OSB, where $\beta_{eff} \cdot p = 0$. According to (1), as S_{11} of the unit cell cannot be zero due to the mismatched structure, all the reflected waves of each unit cell superimpose in phase in the OSB, in which the EM power is barely fed into the SIW structure, which makes the $\alpha_{eff} \cdot p$ considerably large. Therefore, seamless beam scanning through broadside cannot be achieved due to the presence of the OSB.

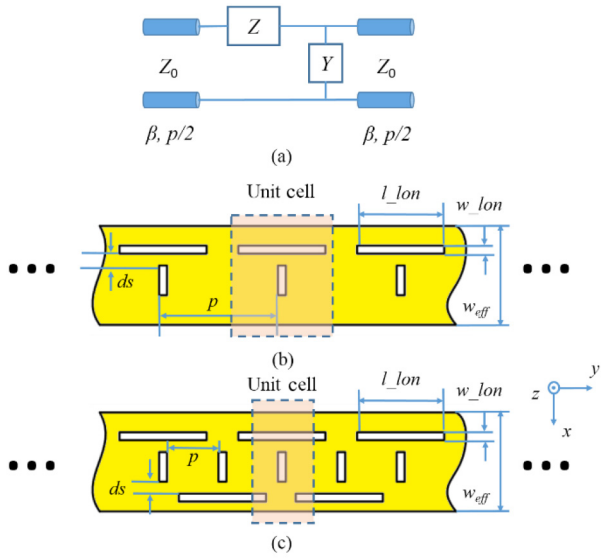

Fig. 5. Structure of LWA with both longitudinal and transverse slots: (a) equivalent circuit of the unit cell; (b) initial design; and (c) modified design.

III. SIW-Based LWA With Continuous Beam Scanning From Backward to Forward

A. Theory Description

As discussed in Section II, SIW-based LWAs with one transverse slot in the unit cell are confronted with the unavoidable emergence of an OSB caused by the severe return loss. The OSB suppression can be achieved by a reflection-canceling unit cell structure, i.e., a radiation element pair with a separation distance of $1/4\ \lambda_g$ [12], [34]. The OSB can be also closed by a transformer in the unit cell for proper impedance tuning [12]. In this section, we try to suppress the OSB by achieving an impedance-matched unit cell structure. As the transverse slot loaded on the SIW only introduces the series impedance Z, a shunt admittance Y cascaded with Z should be added in the equivalent circuit of the unit cell to accomplish impedance matching, as shown in Fig. 5(a). Based on the microwave network theory, the S parameters of the equivalent circuit displayed in Fig. 5(a) can be calculated as follows:

$$\mathrm{S}_{unit} = \begin{pmatrix} S_{11} & S_{21} \\ S_{21} & -S_{11} \end{pmatrix}$$

$$S_{11} = \frac{Z/Z_0 - YZ_0 + ZY}{2 + Z/Z_0 - YZ_0 + ZY} e^{-j\beta p}$$

$$S_{21} = \frac{2}{2 + Z/Z_0 - YZ_0 + ZY} e^{-j\beta p}. \tag{7}$$

According to (7), to achieve impedance matching, i.e., $S_{11} = 0$, Z and Y should follow the relationship described as follows:

$$Y = \frac{Z}{Z_0(Z_0 - Z)}. \tag{8}$$

Furthermore, the real and imaginary parts of the shunt admittance Y are expressed as follows:

$$\begin{cases} \mathrm{Re}[Y] = \dfrac{1}{AZ_0}\left(\dfrac{\mathrm{Re}[Z]}{Z_0}\left(1 - \dfrac{\mathrm{Re}[Z]}{Z_0}\right) + \left(\dfrac{\mathrm{Im}[Z]}{Z_0}\right)^2\right) \\ \mathrm{Im}[Y] = \dfrac{\mathrm{Im}[Z]}{AZ_0}\left(1 - \dfrac{\mathrm{Re}[Z]}{Z_0}\right) \\ A = \left(1 - \dfrac{\mathrm{Re}[Z]}{Z_0}\right)^2 + \left(\dfrac{Im[Z]}{Z_0}\right)^2. \end{cases} \tag{9}$$

It is worth noting that $\mathrm{Re}[Z]/Z_0 \ll 1$ in the frequency band far below the resonant frequency of the slot (see Fig. 2), and hence both of the real and imaginary parts of Y are positive in the band of interest, which renders Y capacitive.

The periodic loading with relatively long longitudinal slots on top of the broad wall of the waveguide can be an effective approach to accomplish parallel capacitive loading in the corresponding equivalent circuit of the unit cell. As longitudinal slots disturb the transverse current of the waveguide, they function as a parallel component, and when properly adjusting its length its resonant frequency drops below the frequency of interest, as expected for capacitive loading. The combination of the proper longitudinal and transverse slots is promising to approximately realize the structure shown in Fig. 5(a).

B. Initial Design

An initial design of the unit cell for a SIW with both transverse and longitudinal slots is illustrated in Fig. 5(b). The longitudinal and transverse slots are aligned like a symmetrical "T" with a distance ds. The length and width of the longitudinal slot are l_lon and w_lon, respectively. The design process consists of two steps: first, the desired frequency for broadside radiation, i.e., the transition frequency, the period of the unit cell should be determined by $\beta \cdot p = 2\pi$ to ensure that adjacent unit cells radiate EM power in phase; second, the parameters of the slots including their sizes and relative position should be properly adjusted to avoid an OSB.

It should be noted that the longitudinal slots are much longer than the transverse slots and hence prone to EM wave radiation, leading to a polarization direction of the proposed LWA in this section that is perpendicular to that of the LWA with only transverse slots. Therefore, and for the sake of a linear polarized LWA, the length of the transverse slots should be reduced to suppress its contribution to the radiation field (cross-polarization).

Comprehensive numerical simulations are conducted to verify all theoretical predictions. All parameter values of the simulation results are listed in Table II. For better physical understanding the mechanism of the proposed unit cell structure, the surface current distribution on the top layer of the unit cell of the initial design is simulated and illustrated in Fig. 6(a). It can be seen that the current distribution around the transverse slot is similar to what is shown in the inset of Fig. 2: it is strong at the slot ends, but weak at the slot center, meaning that the transverse slot is inductive. However, the surface current around the longitudinal slot is strong at the center, but weak at the slot ends. This reversal phenomenon compared to the case of the transverse slot indicates that the longitudinal slot achieves

TABLE II
STRUCTURE PARAMETERS OF THE SIW-BASED LWA WITH TRANSVERSE AND LONGITUDINAL SLOTS

Parameter	Initial design (mm)	Modified design (mm)	Prototype (mm)
w	–	–	10.5
d	–	–	0.8
s	–	–	1.6
w_{eff}	10	10	10
h	0.762	0.762	0.762
ws	0.45	0.45	0.45
Ls	3.5	3.5	4
p	15	7.5	7.5
l_lon	12.2	10	9.5
w_lon	0.45	0.45	0.45
ds	2.5	1	1
N	10	19	19

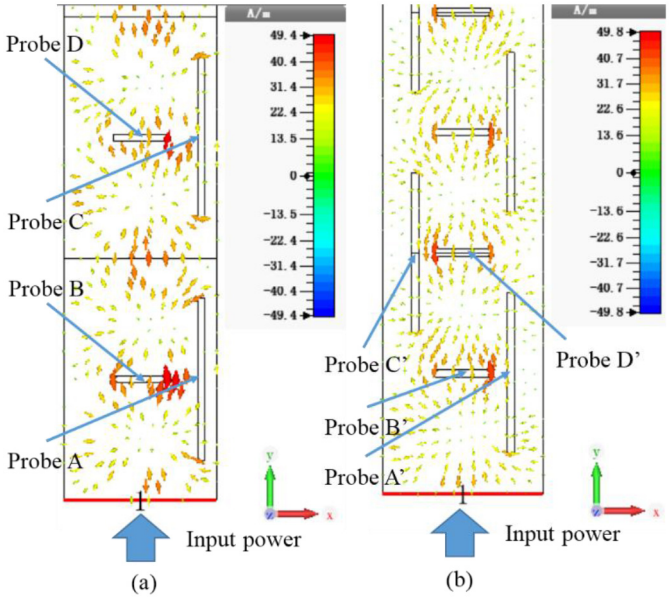

Fig. 6. Simulated surface current distribution on the surface of the (a) initial design and (b) modified design, with *E*-field probes marked.

capacitive loading. Therefore, this unit cell agrees well with the requirements of the equivalent circuit shown in Fig. 5(a).

Both phase delay $|\beta_{eff} \cdot p|$ and attenuation $\alpha_{eff} \cdot p$ of the unit cell of the initial design are depicted in Fig. 7. The decrease and increase of $|\beta_{eff} \cdot p|$ with frequency indicate the backward and forward radiation, respectively. The attenuation of the unit cell is negligible from 9 to 13.8 GHz. The simulated S parameters of the LWA retrieved from the corresponding N cascaded unit cells are depicted in Fig. 8. One can observe that in the total passband, a S_{11} magnitude peak occurs at 11.8 GHz due to the weak OSB effect between the backward radiation band and the forward radiation band. This is because perfect parameter optimization is hard to accomplish (9) for full elimination of the OSB. In fact, the OSB barely affects the broadside radiation as this peak is much lower than -10 dB.

The mainlobe direction and the associated gain of the initial design are illustrated in Fig. 9. As shown, the mainlobe direction of this LWA scans from $-60°$ at 9 GHz to 40° at 14 GHz (undergoing large gain fluctuations), with a maximal realized

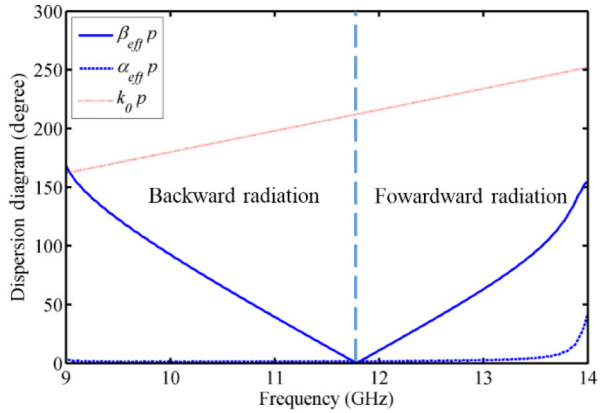

Fig. 7. Simulated dispersion diagram of the unit cell of the LWA with both transverse and longitudinal slots.

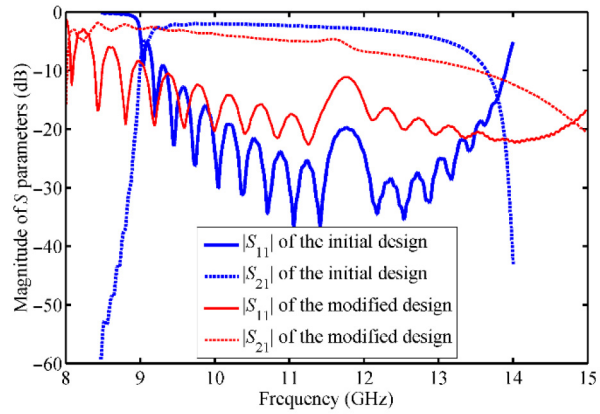

Fig. 8. Simulated spectral response of the magnitude of *S* parameters for both the initial design and the modified design.

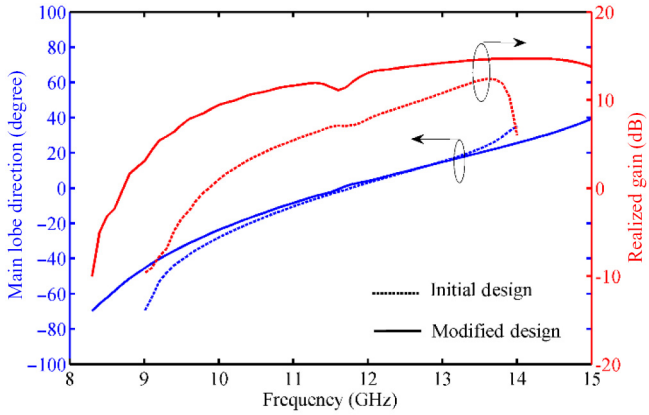

Fig. 9. Mainlobe direction and realized gain of both the initial design and modified design as a function of frequency.

gain of 13.8 dB at 20° (13.2 GHz). Fig. 10(a) plots the mainlobe patterns in the *y–o–z* plane at three typical frequencies. The narrow beam scans smoothly through broadside at the transition frequency of 11.8 GHz, which is consistent with what is shown in Fig. 9. The smooth and steady beam scanning with respect to frequency can be understood by analyzing the phase delay of

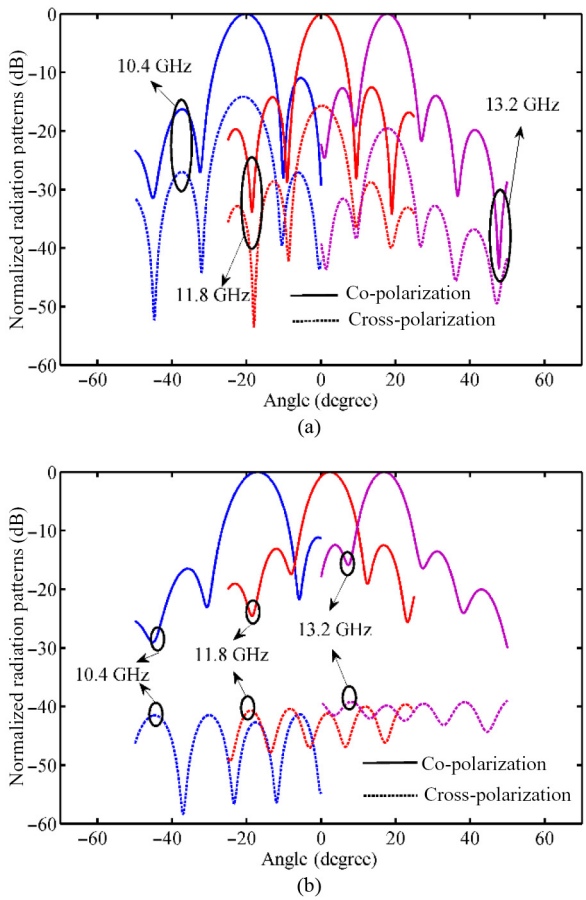

Fig. 10. Simulated frequency-dependent scanning of the mainlobe patterns of the (a) initial LWA design and (b) modified design.

the unit cell. The scattering parameter S_{21} of the unit cell under condition (9) can be rewritten as

$$S_{21} = e^{-j\beta p}. \tag{10}$$

As deduced from (10), the phase delay of one unit cell is only determined by the phase constant β of the host waveguide because the transverse inductive slot and the longitudinal capacitive slot counteract each other and, therefore, do not affect the phase delay of the unit cell. Compared to CRLH LWAs that rely on a cutoff waveguide with a highly dispersive impedance, the proposed LWA makes use of the SIW above the cutoff frequency, resulting in a much steadier frequency behavior.

In summary, the initial design in this section features continuous beam scanning from backward to forward with smooth transition through broadside. The OSB is well suppressed and low return loss is obtained. Although some of its radiation properties need to be improved, such as the low leakage rate in the backward radiation band (see Fig. 9), and the relatively high cross-polarization level (varying from -15 to -20 dB) as shown in Fig. 10(a), the modified design proposed in Section III-C presents a potential solution to these deficiencies.

C. Modified Design

The modified structure is designed as shown in Fig. 5(c). In the modified unit cell, the longitudinal slots are loaded alternately on opposite sides of the transverse slots. For broadside radiation, the phase delay of each unit cell should be reduced to π for the adjacent longitudinal slot to obtain in-phase radiation of the emitted EM power. As a result, the period of the unit cell is reduced by half, yielding radiation contributions from this modified LWA structure that are more densely distributed along the propagation direction (i.e., the y-axis) compared to the initial design. The radiation rate per unit length of the total LWA is, therefore, improved. As the period of the modified unit cell becomes smaller than the length of the longitudinal slots, the coupling between the adjacent unit cells becomes stronger than in the initial design, and thus some parameter adjustment for the modified LWA is needed to suppress a potentially emerging OSB. The parameters of the optimized structure are listed in Table II, and the simulated surface current distribution on the top layer of the unit cell is illustrated in Fig. 6(b), which is similar to the surface current of the initial design. The alternately aligned longitudinal slots give rise to a balanced current distribution with respect to the transverse axis of the SIW on the top layer of the unit cell, which leads to a more symmetrical radiation pattern in the *x–o–z* plane compared to the initial design.

The simulated magnitudes of S parameters as a function of frequency are depicted in Fig. 8. The passband of the modified design approximately overlaps that of the initial design but with broader bandwidth. The peak magnitude of S_{11} in the passband caused by the weak OSB effect appears at the transition frequency of 11.8 GHz. In the modified design the OSB suppression of is harder to achieve compared to the initial design as the $|S_{11}|$ reaches larger values in the passband. As shown in Fig. 8, it is interesting that there is a slight increase of both the $|S_{21}|$ and the $|S_{11}|$ at 11.8 GHz in the modified design, which was also be observed in [23], [26], and [39], where dips in the spectral response of $|S_{21}|$ are more common at transition frequency [4], [25], [26] (which is also true for the initial design). The opposite frequency behavior of the S_{21} magnitude of both the initial design and the modified design reveals the complex effect of the OSB on the reflected power, radiated power, and the remainder power.

The frequency dependence of the simulated mainlobe direction and the associated antenna gain of the modified design are depicted in Fig. 9. In comparison to the results of the initial design, the modified LWA has nearly the same beam scanning range as that of the initial design. This modified LWA reaches its maximum gain of 14.89 dB at 13.7 GHz with a radiation beam pointing at 22.7°. With nearly the same total length, the realized gain of the modified LWA is much higher and its frequency dependence is remarkably steadier compared to the initial design. The mainlobe radiation patterns of the modified LWA at three typical operation frequencies are shown in Fig. 10(b). Continuous beam scanning from backward to forward can be observed. In addition, the resulting cross-polarization level of the modified design is extremely low [better than -40 dB as shown in Fig. 10(b)], much lower than in the initial design. To shed light on this phenomenon, four E-field probes are set at the center of the adjacent slots of both the initial design and the modified design as illustrated in Fig. 6.

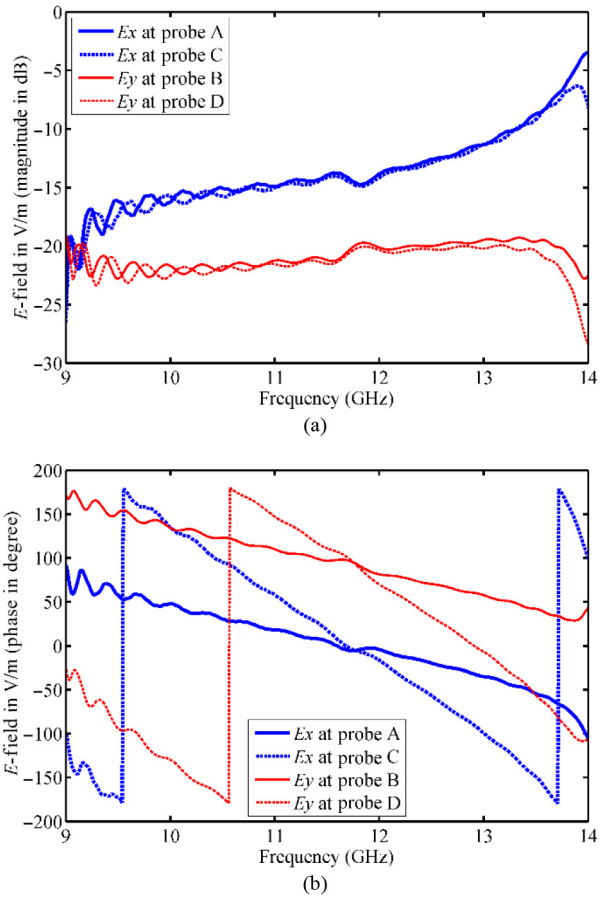

Fig. 11. Simulated spectral response of the (a) normalized magnitude and (b) phase of the *E*-field at the probe set in the initial design.

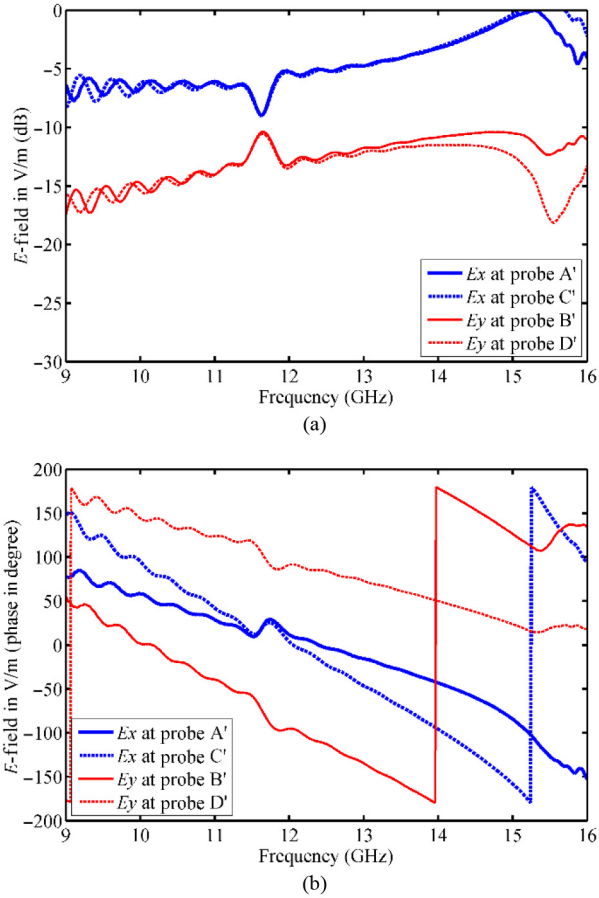

Fig. 12. Simulated spectral response of the (a) normalized magnitude and (b) phase of the *E*-field at the probe set in the modified design.

Fig. 11 depicts the normalized magnitude and phase of the *E*-field at the probes set in the initial design. Probes A and C sense the *E*-field of the adjacent longitudinal slots, while Probes B and D sense the *E*-field of the adjacent transverse slots. As expected, the *E*-field at the longitudinal slots is much stronger than at the transverse slots, making the copolarization direction perpendicular to the longitudinal axis of the SIW as already described in Section III-B. The phase differences of both the adjacent longitudinal slots and the adjacent transverse slots are 2π (i.e., in phase) at the transition frequency of 11.8 GHz. For the case of the modified design, the normalized magnitude and phase of the *E*-field at the probes are plotted in Fig. 12. As shown in Fig. 12(a), similar to the initial design, the *E*-field at the longitudinal slots of the modified design is much stronger than that at the transverse slots. However, the phase differences of the *E*-field of the adjacent transverse slots are only π at the transition frequency as shown in Fig. 12(b), which make the *E*-field excited by the adjacent transverse slots superpose antiphase, but lead to the in-phase superpose of the radiated power of the longitudinal slots as the alternately alignment of the longitudinal slots introduces an additional phase increment of π between the adjacent longitudinal slots. As a result, the cross-polarization level of the modified design is much lower than that of the initial design.

It is interesting to observe that the *E*-field phase difference between the longitudinal and transverse slots is approximately $\pi/2$ at the transition frequency in both the initial design and the modified design. This phenomenon is similar to the case reported in [15]. Therefore, the unit cell composed of both transverse and longitudinal slots is capable to radiate circularly polarized EM wave once the radiated powers of transverse slot and longitudinal slot are balanced. Therefore, the control of the polarization of the proposed SIW-based LWA is more flexible than prior LWA designs constructed from the reflection-canceling units.

IV. Experimental Verification

For verification purposes, we fabricated a prototype of the modified design in Section III as shown in Fig. 13. This prototype is fed by SMA connectors through microstrip-to-SIW transitions [40] as the prototype unit cell is well designed to allow adequate matching to the characteristic impedance of the host SIW. The prototype is fabricated using Rogers 4350 ($\varepsilon_r = 3.66$) substrates. The structure parameters are listed in Table II.

The *S* parameter measurements are conducted using an Agilent N5227A microwave vector network analyzer (VNA), and the results are depicted in Fig. 14, together with the simulation results (from CST MWS). Both simulation and measurement of the magnitude of S_{11} display similar shapes and tendencies in the spectral response. Due to additional

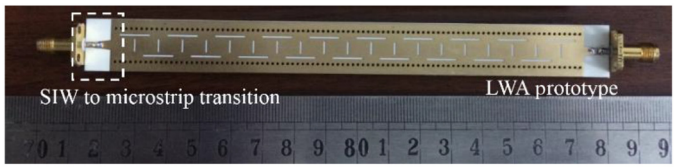

Fig. 13. Realized prototype of the SIW-based LWA.

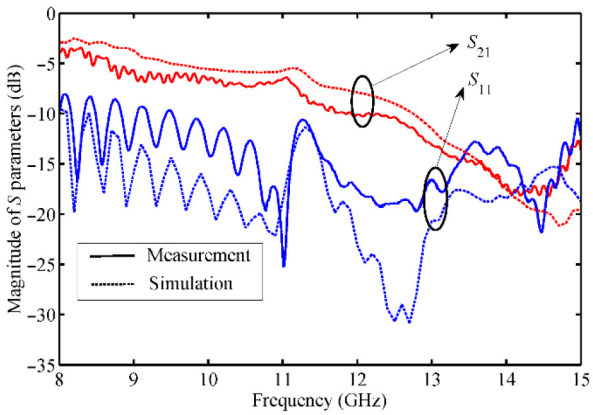

Fig. 14. Measured and simulated magnitude of S parameters of the prototype as a function of frequency.

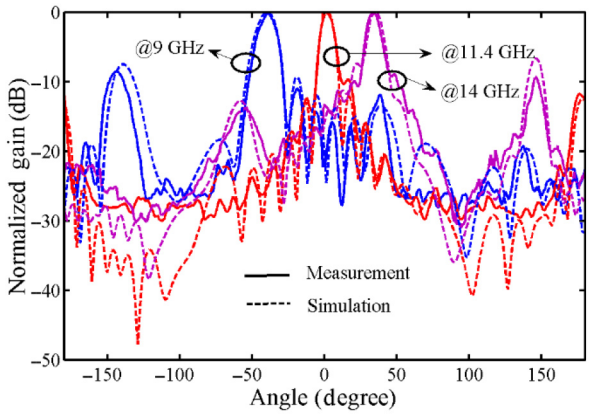

Fig. 15. Measured and simulated radiation patterns of the prototype.

reflections caused by the SMA connectors and potential production variations, the measured $|S_{11}|$ spectrum presents shallower resonance dips compared to the simulated spectrum. Hence, the measured magnitude of the S_{21} prototype's spectral response is also slightly deviating from the corresponding simulated S_{21} spectrum due to the worsened S_{11}.

The measured and simulated normalized radiation patterns of the antenna prototype are depicted in Fig. 15, showing a virtually perfect agreement. The measured and simulated mainlobe direction and associated gain are depicted in Fig. 16. The well agreed measured and simulated results demonstrate that the main radiation beam of the prototype scans at least from $-40°$ at 9 GHz to 35° at 14 GHz with smooth transition through broadside at 11.4 GHz. The maximal realized gain of the prototype is 12 dB.

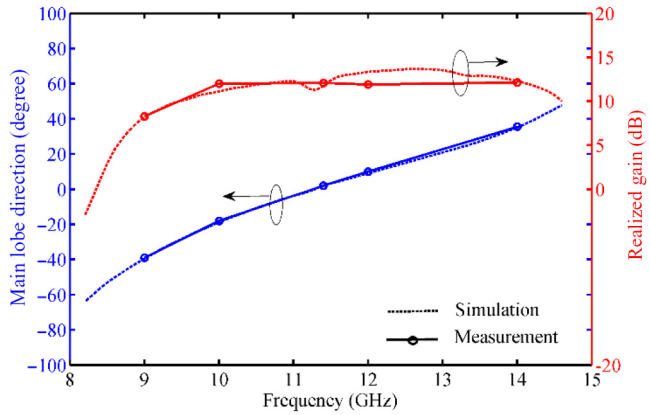

Fig. 16. Mainlobe direction and realized gain of the prototype (both simulation and measurement).

V. Conclusion

In this paper, we have provided a design method for LWAs based on noncutoff SIW supporting continuous beam scanning from backward to forward. First, the radiation mechanisms of the SIW with transverse slots are thoroughly analyzed. Then, with the additional introduction of longitudinal slots, the performance of the original LWA with transverse slots has been significantly improved yielding impedance matching together with the elimination of the OSB between the -1 order backward and forward radiation. This allows a scanning range of the radiation pattern from $-40°$ to 35° with a fractional bandwidth of 55.3%. The proposed LWA operates above cutoff frequency, which is thus easy to feed, and features a smoother beam scanning with regard to frequency compared to a CRLH LWAs that rely on cutoff waveguides. Both simulation and experiment underpin the underlying theory and renders the proposed LWA design very promising for efficient beam steering in ultra-compact millimeter wave antenna applications.

Acknowledgment

The authors would like to thank the reviewers and editors for their constructive comments and suggestions that helped to improve the quality of this paper.

References

[1] A. A. Oliner and D. R. Jackson, *Antenna Engineering Hand Book*, 4th ed. New York, NY, USA: McGraw-Hill, 2007.
[2] R. Hyneman, "Closely-spaced transverse slots in rectangular waveguide," *IRE Trans. Antennas Propag.*, vol. 7, no. 4, pp. 335–342, Oct. 1959.
[3] L. Juhua, D. R. Jackson, and L. Yunliang, "Modal analysis of dielectric-filled rectangular waveguide with transverse slots," *IEEE Trans. Antennas Propag.*, vol. 59, no. 9, pp. 3194–3203, Sep. 2011.
[4] W. Cao, Z. N. Chen, W. Hong, B. Zhang, and A. Liu, "A beam scanning leaky-wave slot antenna with enhanced scanning angle range and flat gain characteristic using composite phase-shifting transmission line," *IEEE Trans. Antennas Propag.*, vol. 62, no. 11, pp. 5871–5875, Nov. 2014.
[5] S. Gupta, S. Abielmona, and C. Caloz, "Microwave analog real-time spectrum analyzer (RTSA) based on the spectral-spatial decomposition property of leaky-wave structures," *IEEE Trans. Microw. Theory Techn.*, vol. 57, no. 12, pp. 2989–2999, Dec. 2009.
[6] A. J. Martinez-Ros, J. L. Gomez-Tornero, V. Losada, F. Mesa, and F. Medina, "Non-uniform sinusoidally modulated half-mode leaky-wave lines for near-field focusing pattern synthesis," *IEEE Trans. Antennas Propag.*, vol. 63, no. 3, pp. 1022–1031, Mar. 2015.

[7] C. Yi-Lin, W. Jin-Wei, H. Jie-Huang, and C. F. Jou, "Design of short microstrip leaky-wave antenna with suppressed back lobe and increased frequency scanning region," *IEEE Trans. Antennas Propag.*, vol. 57, no. 10, pp. 3329–3333, Oct. 2009.
[8] L. Yuanxin, X. Quan, E. K.-N. Yung, and L. Yunliang, "Quasi microstrip leaky-wave antenna with a two-dimensional beam-scanning capability," *IEEE Trans. Antennas Propag.*, vol. 57, no. 2, pp. 347–354, Feb. 2009.
[9] X. Feng, W. Ke, and Z. Xiupu, "Periodic leaky-wave antenna for millimeter wave applications based on substrate integrated waveguide," *IEEE Trans. Antennas Propag.*, vol. 58, no. 2, pp. 340–347, Feb. 2010.
[10] S. Paulotto, P. Baccarelli, F. Frezza, and D. R. Jackson, "Full-wave modal dispersion analysis and broadside optimization for a class of microstrip CRLH leaky-wave antennas," *IEEE Trans. Microw. Theory Techn.*, vol. 56, no. 12, pp. 2826–2837, Dec. 2008.
[11] Y. Li, Q. Xue, E. K.-N. Yung, and Y. Long, "The periodic half-width microstrip leaky-wave antenna with a backward to forward scanning capability," *IEEE Trans. Antennas Propag.*, vol. 58, no. 3, pp. 963–966, Mar. 2010.
[12] S. Paulotto, P. Baccarelli, F. Frezza, and D. R. Jackson, "A novel technique for open-stopband suppression in 1-D periodic printed leaky-wave antennas," *IEEE Trans. Antennas Propag.*, vol. 57, no. 7, pp. 1894–1906, Jul. 2009.
[13] J. T. Williams, P. Baccarelli, S. Paulotto, and D. R. Jackson, "1-D combline leaky-wave antenna with the open-stopband suppressed: Design considerations and comparisons with measurements," *IEEE Trans. Antennas Propag.*, vol. 61, no. 9, pp. 4484–4492, Sep. 2013.
[14] S. Otto, A. Al-Bassam, A. Rennings, K. Solbach, and C. Caloz, "Transversal asymmetry in periodic leaky-wave antennas for Bloch impedance and radiation efficiency equalization through broadside," *IEEE Trans. Antennas Propag.*, vol. 62, no. 10, pp. 5037–5054, Oct. 2014.
[15] S. Otto, C. Zhichao, A. Al-Bassam, A. Rennings, K. Solbach, and C. Caloz, "Circular polarization of periodic leaky-wave antennas with axial asymmetry: Theoretical proof and experimental demonstration," *IEEE Trans. Antennas Propag.*, vol. 62, no. 4, pp. 1817–1829, Apr. 2014.
[16] C. Caloz and T. Itoh, *Electromagnetic Metamaterials: Transmission Line Theory and Microwave Applications: The Engineering Approach*. Hoboken, NJ, USA: Wiley, 2006.
[17] S. Otto, A. Rennings, K. Solbach, and C. Caloz, "Transmission line modeling and asymptotic formulas for periodic leaky-wave antennas scanning through broadside," *IEEE Trans. Antennas Propag.*, vol. 59, no. 10, pp. 3695–3709, Oct. 2011.
[18] L. Wei, C. Zhi Ning, and Q. Xianming, "Metamaterial-based low-profile broadband mushroom antenna," *IEEE Trans. Antennas Propag.*, vol. 62, no. 3, pp. 1165–1172, Mar. 2014.
[19] J. J. Jacome-Munoz, J. S. Gomez-Diaz, J. Perruisseau-Carrier, and A. Alvarez-Melcon, "A tapered CRLH mushroom-like leaky wave antenna with reduced sidelobe level," in *Proc. 8th Eur. Conf. Antennas Propag. (EuCAP'14)*, 2014, pp. 588–592.
[20] M. A. Antoniades and G. V. Eleftheriades, "A CPS leaky-wave antenna with reduced beam squinting using NRI-TL metamaterials," *IEEE Trans. Antennas Propag.*, vol. 56, no. 3, pp. 708–721, Mar. 2008.
[21] A. Mehdipour and G. V. Eleftheriades, "Leaky-wave antennas using negative-refractive-index transmission-line metamaterial supercells," *IEEE Trans. Antennas Propag.*, vol. 62, no. 8, pp. 3929–3942, Aug. 2014.
[22] L. Hong-Min, "A compact zeroth-order resonant antenna employing novel composite right/left-handed transmission-line unit-cells structure," *IEEE Antennas Wireless Propag. Lett.*, vol. 10, pp. 1377–1380, Dec. 19, 2011.
[23] T. Ueda, N. Michishita, M. Akiyama, and T. Itoh, "Dielectric-resonator-based composite right/left-handed transmission lines and their application to leaky wave antenna," *IEEE Trans. Microw. Theory Techn.*, vol. 56, no. 10, pp. 2259–2269, Oct. 2008.
[24] P. Pan, F.-Y. Meng, and Q. Wu, "A composed right/left-handed waveguide with open-ended corrugations for backward-to-forward leaky-wave antenna application," *Microw. Opt. Technol. Lett.*, vol. 50, no. 3, pp. 579–582, Mar. 2008.
[25] K. Dong-Jin and L. Jeong-Hae, "Beam scanning leaky-wave slot antenna using balanced CRLH waveguide operating above the cutoff frequency," *IEEE Trans. Antennas Propag.*, vol. 61, no. 5, pp. 2432–2440, May 2013.
[26] Y. D. Dong and T. Itoh, "Composite right/left-handed substrate integrated waveguide and half mode substrate integrated waveguide leaky-wave structures," *IEEE Trans. Antennas Propag.*, vol. 59, no. 3, pp. 767–775, Mar. 2011.
[27] N. Nasimuddin, Z. N. Chen, and X. M. Qing, "Substrate integrated metamaterial-based leaky-wave antenna with improved boresight radiation bandwidth," *IEEE Trans. Antennas Propag.*, vol. 61, no. 7, pp. 3451–3457, Jul. 2013.
[28] A. Suntives and S. V. Hum, "A fixed-frequency beam-steerable half-mode substrate integrated waveguide leaky-wave antenna," *IEEE Trans. Antennas Propag.*, vol. 60, no. 5, pp. 2540–2544, May 2012.
[29] A. Mallahzadeh and S. Mohammad-Ali-Nezhad, "Long slot ridged SIW leaky wave antenna design using transverse equivalent technique," *IEEE Trans. Antennas Propag.*, vol. 62, no. 11, pp. 5445–5452, Nov. 2014.
[30] S. Mohammad-Ali-Nezhad and A. Mallahzadeh, "Periodic ridged leaky-wave antenna design based on SIW technology," *IEEE Antennas Wireless Propag. Lett.*, vol. 14, pp. 354–357, Feb. 4, 2015.
[31] L. Juhua, D. R. Jackson, and L. Yunliang, "Substrate integrated waveguide (SIW) leaky-wave antenna with transverse slots," *IEEE Trans. Antennas Propag.*, vol. 60, no. 1, pp. 20–29, Jan. 2012.
[32] Y. Mohtashami and J. Rashed-Mohassel, "A butterfly substrate integrated waveguide leaky-wave antenna," *IEEE Trans. Antennas Propag.*, vol. 62, no. 6, pp. 3384–3388, Jun. 2014.
[33] L. Juhua, D. R. Jackson, L. Yuanxin, Z. Chaoqun, and L. Yunliang, "Investigations of SIW leaky-wave antenna for endfire-radiation with narrow beam and sidelobe suppression," *IEEE Trans. Antennas Propag.*, vol. 62, no. 9, pp. 4489–4497, Sep. 2014.
[34] K. Sakakibara, J. Hirokawa, M. Ando, and N. Goto, "A slotted waveguide array using reflection-cancelling slot pairs," in *Proc. IEEE Antennas Propag. Soc. Int. Symp. Dig.*, 1993, vol. 3, pp. 1570–1573.
[35] L. Jae-Ho, T. Hirono, J. Hirokawa, and M. Ando, "A center-feed waveguide transverse slot linear array using a transverse-slot feed for blocking reduction," in *Proc. IEEE Antennas Propag. Soc. Int. Symp.*, 2008, pp. 1–4.
[36] J. Hirokawa and M. Ando, "45° linearly polarised post-wall waveguide-fed parallel-plate slot arrays," *IEE Proc. Microw. Antennas Propag.*, vol. 147, no. 6, pp. 515–519, Dec. 2000.
[37] X. Feng and W. Ke, "Guided-wave and leakage characteristics of substrate integrated waveguide," *IEEE Trans. Microw. Theory Techn.*, vol. 53, no. 1, pp. 66–73, Jan. 2005.
[38] D. M. Pozar, *Microwave Engineering*, 3rd ed. Hoboken, NJ, USA: Wiley, 2004.
[39] J. S. Gomez-Diaz, A. lvarez-Melcon, and T. Bertuch, "A modal-based iterative circuit model for the analysis of CRLH leaky-wave antennas comprising periodically loaded PPW," *IEEE Trans. Antennas Propag.*, vol. 59, no. 4, pp. 1101–1112, Apr. 2011.
[40] D. Deslandes and K. Wu, "Integrated microstrip and rectangular waveguide in planar form," *IEEE Microw. Wireless Compon. Lett.*, vol. 11, no. 2, pp. 68–70, Feb. 2001.

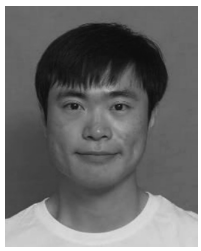

Yue-Long Lyu (S'14) received the B.E. and M.E. degrees in microwave engineering from Harbin Institute of Technology (HIT), Harbin, China, in 2012 and 2014, respectively, where he is currently pursuing the Ph.D. degree in microwave engineering.

His research interests include beam steering antenna, tunable microwave device, and wireless power transfer.

Mr. Lyu was the recipient of the Student Travel Award from the IEEE International Conference on Microwave Magnetics (ICMM), Sendai, Japan, in July 2014, and the Student Paper Contest Award (Honorable Prize) from the 3rd IEEE Asia-Pacific Conference on Antennas and Propagation (APCAP), Harbin, China, in July 2014. He was also awarded as the Outstanding Graduate of HIT in 2012 and 2014, respectively.

Xiao-Xin Liu was born in Tangshan, China, in 1991. He received the B.S. and M.S. degrees in electromagnetic field and microwave technology from Harbin Institute of Technology, Harbin, China, in 2013 and 2015, respectively.

He is currently with Beijing Aerospace Microsystems Institute, Beijing, China. His research interests include the design and measurement of leaky-wave antennas, the design and application of frequency selective surfaces, and RF circuits for broadband wireless communications.

Peng-Yuan Wang received the B.E. degree in communication and information systems from Dalian Maritime University (DLMU), Dalian, China, in 2014. He is currently pursuing the M.E. degree in microwave engineering at Harbin Institute of Technology (HIT), Harbin, China.

His research interests include tunable microwave devices and MIMO system with single RF chain.

Prof. Wang was awarded as the Outstanding Graduate of Dalian in 2014.

Daniel Erni (S'88–M'93) received the Diploma degree in electrical engineering from the University of Applied Sciences (HSR), Rapperswil, Switzerland, in 1986, and the Diploma degree in electrical engineering and the Ph.D. degree in laser physics from ETH Zürich, Zürich, Switzerland, in 1990 and 1996, respectively.

Since 1990, he has been with the Laboratory for Electromagnetic Fields and Microwave Electronics, ETH Zürich. He was the founder, and from 1995 to 2006, the Head of the Communication Photonics Group, ETH Zürich. Since October 2006, he has been a Full Professor of General and Theoretical Electrical Engineering with the University of Duisburg-Essen, Duisburg, Germany. His research interests include advanced data transmission schemes (i.e., O-MIMO) in board-level optical interconnects, optical on-chip interconnects, ultra-dense integrated optics, nanophotonics, plasmonics, quantum optics, and optical and electromagnetic metamaterials; a distinct emphasis on biomedical engineering, namely for advanced RF excitation schemes in magnetic resonance imaging; on the system level, he has pioneered the introduction of numerical structural optimization into dense integrated optics device design; science and technology studies as well as the history and philosophy of science with a distinct focus on the epistemology in engineering sciences.

Dr. Erni is a Member of the Editorial Board of the *Journal of Computational and Theoretical Nanoscience*. He is also a Member of the Center for Nanointegration Duisburg-Essen (CeNIDE), Duisburg, Germany, the Applied Computational Electromagnetics Society (ACES), the Swiss Physical Society (SPS), the German Physical Society (DPG), and the Optical Society of America (OSA). He is an Associated Member of Swiss Electromagnetics Research Centre (SEREC). He is a Fellow of the Electromagnetics Academy.

Qun Wu (M'93–SM'05) received the B.Sc. degree in radio engineering, the M.Eng. degree in electromagnetic fields and microwaves, and the Ph.D. degree in communication and information systems from Harbin Institute of Technology (HIT), Harbin, China, in 1977, 1988, and 1999, respectively.

Since 1990, he has been with the School of Electronics and Information Engineering, HIT, where he is currently a Professor and the Head of the Department of Microwave Engineering. He is also a Director of the Center for Microwaves and EMC, HIT. He was a Visiting Professor at Seoul National University (SNU), Seoul, South Korea, from 1998 to 1999, and Pohang University of Science and Technology, Pohang, South Korea, from 1999 to 2000. He was a Visiting Professor at the National University of Singapore, Singapore, from 2003 to 2010. He has authored several books and more than 100 international and regional refereed journal papers. His research interests include electromagnetic compatibility, metamaterials, and antennas.

Dr. Wu was a Chair or Member with the TPC of international conferences for many times. He is a Vice Chair of the IEEE Harbin Section, and Chair of the IEEE Harbin EMC/AP/MTT Joint Society Chapter. He is a Member of Microwave Society of the Chinese Institute of Electronics. He is a Technical Reviewer for several international journals. He is also invited to give a keynote report or invited papers in some international conferences for many times. He was the recipient of the Science and Technology Award from Heilongjiang Provincial Government in 2010.

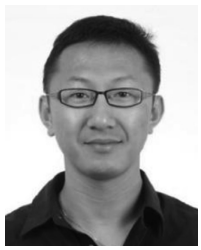

Cong Wang (S'08–M'11–SM'16) was born in Qingdao, Shandong Province, China, in 1982. He received the B.S. degree in automation engineering from Qingdao Technological University, Qingdao, China, in 2005, and the M.S. and Ph.D. degrees in electronic engineering from Kwangwoon University, Seoul, South Korea, in 2008 and 2011, respectively.

In 2007, he was a Research Engineer with the R&D Department, Mission Technology Co., Ltd., Gyeonggi-do, South Korea, where he was involved in the development of microwave components and devices using hybrid and LTCC technology. He joined R&D Department, NanoENS Co., Ltd., Gyeonggi-do, South Korea, in 2007. He is currently with Kwangwoon University as an Assistant Professor, working on passive device modeling, passive device design, and fabrication process development and optimization. He has co-authored 2 books and published more than 190 papers in domestic and international journals and conference proceedings. He has also more than 40 patents registered in South Korea. His research interests include RFIC/MMIC design and semiconductor fabrication development such as GaAs integrated passive device, silicon-based LED module fabrication and packaging, AlGaN/GaN HEMT, and various kinds of smart sensors and their applications which are emerging technologies of today.

Nam-Young Kim (M'10) received the Master's and Ph.D. degrees in electronic engineering from the State University of New York (SUNY), Buffalo, NY, USA, in 1991 and 1994, respectively, and the Master's and Ph.D. degrees in theology from the Midwest University, St. Louis, MO, USA, in 2004 and 2006, respectively.

He was a Research Scientist with the Center for Electronic and Electrooptic Materials (CEEM), SUNY at Buffalo. In 1994, he joined the Department of Electronic Engineering, Kwangwoon University, Seoul, Korea, as a Professor. His main research focus is RF integrated circuits(RFICs), RF nano-devices, and RF nano-bio devices. He is the founder of the RFIC Research Center and also serves as Director of the Fusion Technology Center, Kwangwoon University. He leads the RFIC and MMIC compound semiconductor related research group at Kwangwoon University. He has authored or coauthored for 555 refereed journal papersand refereed conference papers, and 28 books. He holds over 115 patents and 200 semiconductor design patents. His research field is RFIC, MMIC, LED Modules, RF Bio Sensor and RF Nono devices.

Fan-Yi Meng (S'07–M'09–SM'15) received the B.S., M.S., and Ph.D. degrees in electromagnetics from Harbin Institute of Technology, Harbin, China, in 2002, 2004, and 2007, respectively.

Since August 2007, he has been with the Department of Microwave Engineering, Harbin Institute of Technology, where he is currently a Professor. He has coauthored 4 books, 50 international refereed journal papers, more than 20 regional refereed journal papers, and 30 international conference proceedings. His research interests include antennas, electromagnetic and optical metamaterials, plasmonics, and electromagnetic compatibility (EMC).

Dr. Meng was the recipient of several awards including the 2013 Top Young Innovative Talents of Harbin Institute of Technology, the 2013 CST University Publication Award, the 2010 Award of Science and Technology from the Heilongjiang Province Government of China, the 2010 "Microsoft Cup" IEEE China Student Paper Contest Award, two Best Paper Awards from the National Conference on Microwave and Millimeter Wave in China in 2009 and 2007, respectively, the 2008 University Excellent Teacher Award of the National University of Singapore, the 2007 Excellent Graduate Award of Heilongjiang Province of China, and the Outstanding Doctor Degree Dissertation Award of the Harbin Institute of Technology.